J. Fluid Mech. (1985), *vol.* 155, *pp.* 193–212
Printed in Great Britain

Effects of density change and subcooling on the melting of a solid around a horizontal heated cylinder

By J. PRUSA
Department of Mechanical Engineering, Iowa State University, Ames, Iowa 50011

AND L. S. YAO
Department of Mechanical and Aerospace Engineering, Arizona State University, Tempe, Arizona 85203

(Received 2 April 1984 and in revised form 7 December 1984)

The unsteady two-dimensional heat-transfer problem of melting around a horizontal heated cylinder is studied numerically. The cylinder is heated isothermally. A physical model is introduced which accounts for the effects of density change upon melting and subcooling effect, as well as natural convection. Most previous work has assumed that the density number (ratio of solid density to liquid density) is unity. In practice, all solid materials exhibit some density change upon melting. If the density number is greater than one, this induces a blowing effect at the phase-change boundary. If the density number is less than one, a suction effect is produced. This study indicates that the density-change effect on heat transfer during melting is minor. Subcooling results when the solid is at a temperature below the melting temperature. When the melting process begins, some of the available thermal energy must be used as sensible heat, to raise the solid's temperature to the melting point. As a result, less thermal energy is available for melting. Subcooling effects are found to have a substantial effect on the heat-transfer process. The effects of natural convection have been clearly documented, and indicate that natural convection must be included in any realistic model of the melting process. Detailed predictions of the effects of density change and subcooling on the melting process are given. Information on the temperature and flow fields for representative values of Stefan, Rayleigh, Prandtl, subcooling and density number is given. Further results from the numerical solutions include information on local and average heat-transfer rates and sensible-heat gain as well as melt volume as a function of time. Comparisons are made with earlier numerical and analytical results.

1. Introduction

Heat transfer with solid–liquid phase-change is encountered often in modern technology. Examples range from the solidification of castings, to ice formation and melting, and the ablation of surfaces due to aerodynamic heating (e.g. spacecraft re-entry). More examples are found in the purification of materials, in the freeze drying of foodstuffs, and in geophysics. Solid–liquid phase-change problems involved in low- and moderate-temperature thermal-storage systems are also of keen interest in our energy-conscious world. Typically, these thermal-storage problems occur in

solar-energy applications and in spacecraft thermal-control systems. This study solves the problem of melting about an isothermally heated horizontal cylinder.

Initially, the horizontal cylinder is completely surrounded by solid phase-change-material (PCM). At time zero, the cylinder surface temperature is suddenly raised above the melting point of the PCM, and heat transfer from the cylinder to the PCM begins. Instantaneously, an infinitesimal melt region forms. This sudden appearance of liquid phase introduces a singularity into the governing equations at time zero (Carslaw & Jaeger 1962; Rubenstein 1971). The singularity is removed by using appropriate scales for the dependent variables. If this is not done, an *ad hoc* starting method must be used which begins the computation away from time zero. The errors which such methods introduce are discussed in Prusa & Yao (1984*b*).

Since the melt volume increases with time, the position of the liquid–solid interface is unknown *a priori* for times greater than zero. The interface is consequently another dependent variable in the problem. Complicating matters even further are the effects of natural convection in the melt region. Such effects have been observed experimentally by Bathelt, Viskanta & Leidenfrost (1979), Sparrow, Schmidt & Ramsey (1978) and Goldstein & Ramsey (1979). In these studies, the melting region grew most rapidly above the heated horizontal cylinder. This produced an elongated melt region with the heated cylinder towards the bottom. The melt region appeared symmetrical with respect to the vertical. Natural convection, driven by the change in fluid density due to temperature gradients in the melt region, forms two antisymmetric vortices. The local heat-transfer rate along the interface is maximum at the top of the melt region, where a thermal plume impinges. This causes the higher rate of melting at the top of the melt region. The effect of natural convection in producing a non-uniform interface has also been demonstrated analytically by Yao & Chen (1980), and Yao & Cherney (1981); and numerically by Ramachandran, Gupta & Jaluria (1982), Saitoh & Hirose (1982), Rieger, Projahn & Beer (1982), Sparrow, Patankar & Ramadhyani (1977) and Prusa & Yao (1984*a*). This non-uniform moving boundary is handled in the present study by using a coordinate-transformation method (Yao & Chen 1980; Yao & Cherney 1981; Sparrow *et al.* 1977; Prusa 1983) to generate a natural coordinate system which is precisely aligned with it.

Although it is generally becoming recognized in the heat-transfer community that natural convection has important effects upon the melting process, the effects of subcooling and density change upon melting are still largely unknown and ignored. Yao & Cherney (1981) determined a short-time solution – incorporating subcooling – for the melting of a solid about a heated horizontal cylinder. Using an integral method, the solution is based upon the insight that, for a small interval of time after the start of melting, conduction is the dominant mode of heat transfer. Although the length of this interval depends upon several factors, a criterion which may be used to define it is the initial interval of time during which local heat-transfer rates are uniform. Subcooling was found to reduce the rate of melting and suppress natural-convection heat transfer. This occurs because some of the thermal energy which is available must be used to raise the solid PCM temperature to the melting point. This effect is enhanced if the thermal diffusivity of the solid is greater than the thermal diffusivity of the liquid because the solid is then able to diffuse thermal energy away more quickly. Yao & Cherney's solution indicates that the subcooling effect can be quite large – up to a 50% reduced melting rate – in this initial interval of time. No information on the subcooling effect is available for times beyond the initial interval for which the integral solution is valid. The effects of density change upon melting are even less well known than subcooling effects. Ho & Viskanta (1982) experimentally

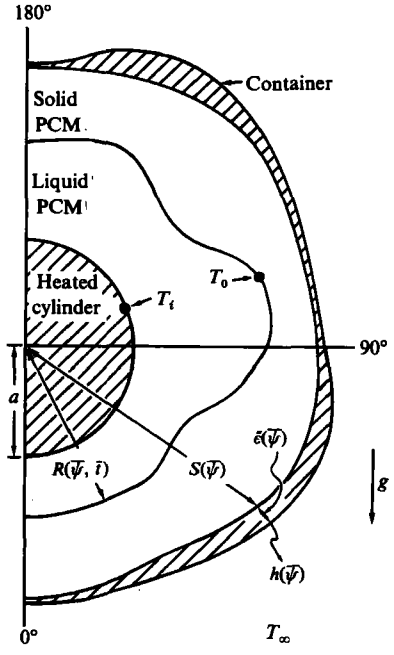

FIGURE 1. Physical model for melting problem.

detected fluid motions early in the melting process in a rectangular cell. They attributed it to the density change that accompanies phase transformation. Epstein & Cheung (1983) also mention the importance of refining models for melting so that the effects of density change can be incorporated. No results on these effects are mentioned, however.

The present work is motivated by interest in demonstrating the effects of subcooling and density change on the melting of a solid PCM. A numerical method is used to determine the solution, which is valid over any arbitrary interval of time. Consequently, the effects of subcooling can be determined throughout the melting process, well beyond the initial interval in which conduction is the dominant mode of heat transfer.

2. Analysis

The physical model considers a horizontal heated tube which is embedded in solid PCM. The heated tube is in an arbitrarily shaped shell which contains the PCM (see figure 1). The tube and containing shell are infinite in their axial extent. Using polar coordinates, the independent variables are then radius $\bar{r}$, angular coordinate $\bar{\psi}$, and time $\bar{t}$. The heated tube has its radius denoted by a, while the inner radius of the containing shell is denoted by $S(\bar{\psi})$. $\bar{\epsilon}(\bar{\psi})$ denotes the thickness of the shell. A convective boundary condition is used along the outside of the shell. The solid PCM is originally at a uniform temperature of T_∞, which may be below the melting temperature T_0. The ambient atmosphere surrounding the shell is also at temperature T_∞. At time zero, the heated cylinder's surface temperature suddenly increases to temperature T_i, which is greater than T_0, and the melting process begins. As solid PCM melts, its density may increase, decrease or remain unchanged.

A vorticity-stream-function approach is used to model the fluid motion in the melt

region. The stream-function is defined so that the continuity equation is satisfied identically:

$$\bar{u} = -\frac{1}{\bar{r}}\frac{\partial \bar{f}}{\partial \bar{\psi}} \quad \text{and} \quad \bar{v} = \frac{\partial \bar{f}}{\partial \bar{r}},$$

where $\bar{u}$ and $\bar{v}$ are the radial and angular components of velocity. The change in stream function between two points in the flow field can be seen to be equal to the volume flow rate between these two points. All material properties are considered constant, with the exception of liquid-PCM density, which is allowed to vary in the buoyancy terms of the momentum equations. The unsteady fluid motion induced by buoyancy force is assumed to be laminar. The dependent variables are liquid-PCM temperature $\bar{T}_1$, vorticity $\bar{\omega}$, stream function $\bar{f}$, and solid-PCM temperature $\bar{T}_s$; they are all functions of the independent variables $\bar{r}$, $\bar{\psi}$ and $\bar{t}$. These dependent variables may be determined by solving the following system of simultaneous governing equations:

$$\frac{\partial \bar{\omega}}{\partial \bar{t}} + \frac{1}{\bar{r}}\frac{\partial(\bar{f}, \bar{\omega})}{\partial(\bar{r}, \bar{\psi})} = \nu \nabla^2 \bar{\omega} - g\beta\left(\sin\bar{\psi}\frac{\partial \bar{T}}{\partial \bar{r}} + \frac{\cos\bar{\psi}}{\bar{r}}\frac{\partial \bar{T}}{\partial \bar{\psi}}\right); \tag{1a}$$

$$\frac{\partial \bar{T}_1}{\partial \bar{t}} + \frac{1}{\bar{r}}\frac{\partial(\bar{f}, \bar{T}_1)}{\partial(\bar{r}, \bar{\psi})} = \alpha_1 \nabla^2 \bar{T}_1; \tag{1b}$$

$$\nabla^2 \bar{f} = -\bar{\omega}; \quad \frac{\partial \bar{T}_s}{\partial \bar{t}} = \alpha_s \nabla^2 \bar{T}_s; \tag{1c, d}$$

where $$\nabla^2 = \frac{\partial^2}{\partial \bar{r}^2} + \frac{1}{\bar{r}}\frac{\partial}{\partial \bar{r}} + \frac{1}{\bar{r}^2}\frac{\partial^2}{\partial \bar{\psi}^2} \quad \text{and} \quad \frac{\partial(P, Q)}{\partial(x, y)} = \frac{\partial P}{\partial x}\frac{\partial Q}{\partial y} - \frac{\partial P}{\partial y}\frac{\partial Q}{\partial x}.$$

Equation (1*a*) represents conservation of vorticity in the viscous flow of liquid PCM, (1*b*) is conservation of thermal energy in the liquid PCM while (1*d*) is conservation of thermal energy in the solid PCM. Equation (1*c*) may be considered to be the definition of the streamfunction. ν, β and α_1 are the kinematic viscosity, the coefficient of expansion, and the thermal diffusivity, respectively, of the liquid PCM; α_s is the thermal diffusivity of the solid PCM; g is the local acceleration of gravity. Note that the buoyancy-force term in (1*a*) is approximated by the Boussinesq form. Therefore the change in density which produces the buoyancy force must satisfy $\Delta\rho_1/\rho_1 \ll 1$ to ensure the validity of the solution. ρ_1 denotes the density of the liquid PCM. The Jacobian terms represent convection effects while the ∇^2 operator represents diffusion effects in (1*a–d*).

2.1. *Liquid–solid interface location*

The radius of the liquid–solid interface R is the fifth dependent variable in the phase-change problem. A governing equation can be determined for it by considering an energy balance in a control system at the interface. The result is found to be:

$$\dot{R} = -\frac{k_1}{\rho_s h_{sl}}\left(\frac{\partial \bar{T}_1}{\partial \bar{r}} - \frac{R'}{R^2}\frac{\partial \bar{T}_1}{\partial \bar{\psi}}\right)\Bigg|_{\bar{r}=R} + \frac{k_s}{\rho_s h_{sl}}\left(\frac{\partial \bar{T}_s}{\partial \bar{r}} - \frac{R'}{R^2}\frac{\partial \bar{T}_s}{\partial \bar{\psi}}\right)\Bigg|_{\bar{r}=R}, \tag{1e}$$

where $$\dot{R} = \frac{\partial R}{\partial \bar{t}} \quad \text{and} \quad R' = \frac{\partial R}{\partial \bar{\psi}}.$$

k_1 and k_s are the liquid- and solid-phase thermal conductivities, respectively, ρ_s is the solid-PCM density and h_{sl} is the latent heat of fusion. Conduction heat transfer through the liquid–solid interface occurs in a direction normal to it as it is isothermal

(at the melting temperature). Since the interface between the liquid and solid phases is not necessarily a circle centred on the pole, rays of constant $\bar{\psi}$ are not generally normal to it. The appearance of the $\partial\bar{T}/\partial\bar{\psi}$ terms in (1*e*) is the direct result of this. The first term in parenthesis represents conduction in the liquid, while the second term gives the solid heat-conduction effect. The vorticity, streamfunction and energy equations for the liquid and solid PCM provide sufficient governing equations, when coupled with (1*e*), to determine all of the dependent variables.

2.2. *Initial conditions*

At time $\bar{t} = 0^+$, the heating of the solid phase begins. Instantaneously, a concentric annular melt region of infinitesimal thickness appears around the heated cylinder. This sudden appearance of liquid phase corresponds to a singularity in the governing equations at time zero. In the initial conditions, this is manifested in the form of temperature discontinuities:

$$T_i \geqslant \bar{T}_l \geqslant T_0 \quad \text{at } \bar{r} = a; \tag{2a}$$

$$\bar{T}_s = T_0 \quad \text{at } \bar{r} = a \quad \text{and} \quad \bar{T}_s = T_\infty \quad \text{for } \bar{r} > a; \tag{2b}$$

$$\bar{\omega} \equiv \bar{f} \equiv 0 \quad \text{if } \frac{\rho_s}{\rho_l} = 1 \quad \text{or} \quad \bar{\omega} \text{ and } \bar{f} \text{ are unbounded} \quad \text{if } \frac{\rho_s}{\rho_l} \neq 1; \tag{2c}$$

$$R \equiv a. \tag{2d}$$

It is interesting to observe that, if a change in density occurs during melting, the blowing or suction velocity which results must become unbounded as $\bar{t} \to 0$. This accounts for the unusual initial condition for $\bar{\omega}$ and $\bar{f}$. That this is actually correct can be observed by examining the initial singularities which exist in the governing equations and boundary conditions at time zero.

2.3. *Boundary conditions*

Along the heated cylinder, a no-slip boundary condition leads to the traditional formulation for vorticity and stream function (Roache 1976). Along the interface, however, the hydrodynamic boundary conditions are complicated both by the non-uniform growth and by the blowing or suction effect caused by density change during melting.

If there is no density change during melting, then the fluid velocity at the interface is zero. The PCM does not move along with the interface. Physically, solid PCM at the interface is motionless as it is melted (Yang 1972). The liquid PCM which results is also momentarily motionless until the hydrodynamic boundary layer which is following the interface passes it by.

If a density change does occur, then a non-zero velocity results at the interface. A mass balance on a control volume at the interface demonstrates that the interface velocity is:

$$\overline{u_R} = \dot{R}\left(1 - \frac{\rho_s}{\rho_l}\right) \Big/ \left(1 + \frac{R'^2}{R^2}\right) \quad \text{(radial component)}; \tag{3a}$$

$$\overline{v_R} = \overline{u_R}\,\frac{R'}{R} \quad \text{(angular component)}. \tag{3b}$$

The interface boundary condition for the stream function can now be determined in terms of the interface velocity if it is remembered that the change in stream function

between two points equals the volume flow rate. The boundary conditions for the liquid region can now be summarized as:

$$\bar{T}_1 = T_i, \quad \bar{f} = 0, \quad \bar{\omega} = -\frac{\partial^2 \bar{f}}{\partial \bar{r}^2} \quad \text{at } \bar{r} = a; \tag{4a}$$

$$\bar{T}_1 = T_0 \quad \text{at } \bar{r} = R; \tag{4b}$$

$$\left.\frac{\partial \bar{f}}{\partial \bar{s}}\right|_R = \left\{\frac{R'}{R}\bar{v}_R - \bar{u}_R\right\} \Big/ \left(1 + \frac{R'^2}{R^2}\right)^{\frac{1}{2}} \quad \text{(tangential gradient along the interface)}; \tag{4c}$$

$$\bar{\omega} = -\nabla^2 \bar{f} \quad \text{at } \bar{r} = R \text{ (all terms retained)} \tag{4d}$$

The thickness of the container wall is assumed to be small in comparison to its radius so that a linear temperature distribution can be used for it. Both the inner radius of the container wall S and the wall thickness $\bar{\epsilon}$ may be arbitrary functions of $\bar{\psi}$. A convective boundary condition with a specified value of convection coefficient $h(\bar{\psi})$ is used on the outside surface. On the inside surface of the container, the temperature and local heat flux are matched between solid PCM and container material. The boundary conditions for the solid region can now be summarized as:

$$\bar{T}_s = T_0 \quad \text{at } \bar{r} = R; \tag{5a}$$

and

$$\frac{\partial \bar{T}_s}{\partial \bar{r}} - \frac{S'}{S^2}\frac{\partial \bar{T}_s}{\partial \bar{\psi}} = -\frac{k_w}{k_s}\frac{h}{k_w + \bar{\epsilon}h}\left(1 + \frac{S'^2}{S^2}\right)^{\frac{1}{2}}\left(\bar{T}_s - T_\infty\right) \quad \text{at } \bar{r} = S. \tag{5b}$$

k_w denotes the thermal conductivity of the container wall.

2.4. *Dimensionless formulation for liquid region*

The radial coordinate in the liquid region is non-dimensionalized so that the outer boundary formed by the liquid–solid interface, at $\bar{r} = R$, is transformed into the unit circle, $r_1 = 1$. The inner boundary, $\bar{r} = a$, is transformed into the pole, $r_1 = 0$. This constitutes the coordinate transformation. In dimensionless form, the radial distance from the inner cylinder to the interface is measured by the gap function Z. When the cylinder is heated so as to maintain a constant surface temperature, a singularity in the governing equations at time zero appears which is of order $t^{\frac{1}{2}}$. Consequently, to remove it from the governing equations, $t^{\frac{1}{2}}$ is factored out of the gap function. The coordinate transformation then takes on the following form:

$$r_1 = \frac{\bar{r} - a}{aZ(2t)^{\frac{1}{2}}}, \quad \psi = \bar{\psi}, \quad t = \frac{\bar{t}}{a^2/\alpha_1} \quad \text{(coordinates)}; \tag{6a}$$

$$Z = \frac{R - a}{a(2t)^{\frac{1}{2}}} \quad \text{(gap function)}. \tag{6b}$$

If the PCM changes density upon melting, then additional singularities appear in the governing equations at time zero. Since these singularities are present only when there is initial fluid motion (due to density change), we will term them convection singularities. The convection singularity for the streamfunction is also of order $t^{\frac{1}{2}}$, that is, the stream function becomes unbounded like $t^{-\frac{1}{2}}$ as $t \to 0$. The convection singularity for vorticity is of order $t^{\frac{3}{2}}$. Consequently, vorticity becomes unbounded much faster than the stream function as $t \to 0$. In order to remove these convection singularities, $t^{\frac{1}{2}}$ and $t^{\frac{3}{2}}$ are factored out of the dimensionless stream function and vorticity. The

temperature is scaled using the temperature difference between the heated cylinder and the melting temperature. The following dimensionless variables result:

$$f=\frac{\bar{f}(2t)^{\frac{1}{2}}}{\alpha_1};\quad \omega=\frac{\bar{\omega}(2t)^{\frac{3}{2}}}{\alpha_1/a^2};\quad T_1=\frac{\bar{T}-T_0}{T_i-T_0}; \tag{6c–e}$$

$$Pr=\frac{\nu}{\alpha_1}\ \text{(Prandtl number)};\quad Ra=\frac{g\beta a^3(T_i-T_0)}{\nu\alpha_1}\ \text{(Rayleigh number)}. \tag{6f,g}$$

Equations (6*a–e*) are substituted into the dimensional governing equations for the melt region and, after some algebraic simplification, the following dimensionless governing equations result:

$$\frac{1}{Pr}\left\{2tZ^2\left(\frac{\partial\omega}{\partial t}-\frac{3\omega}{2t}\right)-r_1(2tZ\dot{Z}+Z^2)\frac{\partial\omega}{\partial r_1}+\frac{Z}{1+r_1Z(2t)^{\frac{1}{2}}}\frac{\partial(f,\omega)}{\partial(r_1,\psi)}\right\}$$
$$=(\nabla_1^2-\mathrm{N}_1)\,\omega-4Zt^2\,Ra\left\{\frac{\cos\psi}{r_1+1/Z(2t)^{\frac{1}{2}}}\frac{\partial T_1}{\partial\psi}+\left(\sin\psi-\frac{r_1Z'\cos\psi}{r_1Z+1/(2t)^{\frac{1}{2}}}\right)\frac{\partial T_1}{\partial r_1}\right\}; \tag{7a}$$

$$2tZ^2\frac{\partial T_1}{\partial t}-r_1(2tZ\dot{Z}+Z^2)\frac{\partial T_1}{\partial r_1}+\frac{Z}{1+r_1Z(2t)^{\frac{1}{2}}}\frac{\partial(f,T_1)}{\partial(r_1,\psi)}=(\nabla_1^2-\mathrm{N}_1)\,T_1; \tag{7b}$$

$$(\nabla_1^2-\mathrm{N}_1)f=-Z^2\omega; \tag{7c}$$

where

$$\nabla_1^2=\frac{\partial^2}{\partial r_1^2}+\frac{1}{r_1+1/Z(2t)^{\frac{1}{2}}}\frac{\partial}{\partial r_1}+\frac{1}{(r_1+1/Z(2t)^{\frac{1}{2}})^2}\frac{\partial^2}{\partial\psi^2};$$

$$\mathrm{N}_1=\frac{1}{(r_1+1/Z(2t)^{\frac{1}{2}})^2}\left\{\frac{2r_1Z'}{Z}\frac{\partial^2}{\partial r_1\partial\psi}+\left(\frac{Z''}{Z}-\frac{2Z'^2}{Z^2}\right)r_1\frac{\partial}{\partial r_1}-\frac{r_1^2Z'^2}{Z^2}\frac{\partial^2}{\partial r_1^2}\right\};$$

$$\frac{\partial(P,Q)}{\partial(x,y)}=\frac{\partial P}{\partial x}\frac{\partial Q}{\partial y}-\frac{\partial P}{\partial y}\frac{\partial Q}{\partial x};$$

$$Z'=\frac{\partial Z}{\partial\psi},\quad Z''=\frac{\partial^2Z}{\partial\psi^2},\quad \text{and } \dot{Z}=\frac{\partial Z}{\partial t}.$$

Note the appearance of the differential operator N_1. It represents the effects of the irregular curvature of the interface. N_1 vanishes if the interface is a circle centred on the pole. The implicit partial differentiation of the transformation also causes a second type of term to appear in the dimensionless equations. This is the $r\,\partial/\partial r$ term which appears on the left-hand sides of (7*a*, *b*). This term introduces the effects of the movement of the interface into the dimensionless governing equations. On the right-hand side of the conservation of vorticity equation (7*a*) a vorticity source term appears. It originates from the unsteady term and appears because of the convective singularity in vorticity at time zero.

The dimensionless boundary conditions are found by substitution of the dimensionless variables into the dimensional boundary conditions:

$$T_1=1,\quad f=0,\quad \omega=-\frac{1}{Z^2}\frac{\partial^2 f}{\partial r_1^2}\quad \text{at } r_1=0; \tag{8a}$$

$$\left.\begin{aligned} &T_1=0,\quad \frac{\partial f}{\partial\psi}=Z'(2t)^{\frac{1}{2}}v_R-[1+Z(2t)^{\frac{1}{2}}]\,u_R,\\ \text{and}\quad &\omega=-\frac{1}{Z^2}\left\{1+\frac{Z'^2}{(Z+(2t)^{-\frac{1}{2}})^2}\right\}\frac{\partial^2 f}{\partial r_1^2}-2t\omega^*\quad \text{at } r_1=1; \end{aligned}\right\} \tag{8b}$$

where
$$\omega^* = \omega^*(Z, Z', Z'', v_R, v_R', u_R, u_R', t), \tag{8c}$$

$$u_R = \overline{u_R}\frac{(2t)^{\frac{1}{2}}}{\alpha_1/a} = (2t\dot{Z}+Z)(1-\Delta)\left\{1+\left(\frac{2tZ'^2}{1+Z(2t)^{\frac{1}{2}}}\right)^2\right\}^{-1}, \tag{8d}$$

$$v_R = \overline{v_R}\frac{(2t)^{\frac{1}{2}}}{\alpha_1/a} = -\frac{2tZ'u_R}{1+Z(2t)^{\frac{1}{2}}}, \tag{8e}$$

and
$$\Delta = \rho_s/\rho_1. \tag{8f}$$

2.5. *Dimensionless formulation for solid region*

The radial coordinate in the solid region is non-dimensionalized so that the inner boundary formed by the liquid–solid interface, at $\bar{r} = R$, is transformed into the unit circle, $r_s = 1$. The outer boundary, $\bar{r} = S$, is transformed into the pole $r_s = 0$. This coordinate transformation is completely analogous to the one used for the melt region. In dimensionless form, the radial distance from the solid–liquid interface to the outer shell is measured by the gap function C. The coordinate transformation for the solid region is then:

$$r = \frac{S-\bar{r}}{aC}, \quad \psi = \overline{\psi}, \quad t = \frac{\bar{t}}{a^2/\alpha_1} \quad \text{(coordinates)}; \tag{9a}$$

$$C = (S-R)/a \quad \text{(gap function)}. \tag{9b}$$

We scale the dimensionless solid temperature using the temperature difference between the melt temperature and the ambient temperature. For the solid PCM, the appropriate dimensionless variables are:

$$T_s = \frac{\overline{T}-T_\infty}{T_0-T_\infty}; \quad Bi = \frac{ha}{k_s} \quad \text{(Biot number)}; \tag{9c–d}$$

$$K = \frac{k_s}{k_w}; \quad \epsilon = \frac{\bar{\epsilon}}{a}; \quad \lambda = \frac{\alpha_s}{\alpha_1}; \quad \Sigma = \frac{S}{a} = 1+Z(2t)^{\frac{1}{2}}+C. \tag{9e–h}$$

The conservation-of-energy equation for the solid region is non-dimensionalized using (9) with the following result:

$$C^2\frac{\partial T_s}{\partial t} - r_s C\dot{C}\frac{\partial T_s}{\partial r_s} = \lambda(\nabla_2^2 - \mathrm{N}_2)T_s, \tag{10a}$$

where
$$\nabla_2^2 = \frac{\partial^2}{\partial r_s^2}+\frac{1}{(r_s-\Sigma/C)}\frac{\partial}{\partial r_s}+\frac{1}{(r_s-\Sigma/C)^2}\frac{\partial^2}{\partial \psi^2};$$

$$\mathrm{N}_2 = \frac{1}{(r_s-\Sigma/C)^2}\left\{\frac{2r_sC'}{C}\frac{\partial^2}{\partial r_s\partial\psi}+\left(\frac{C''}{C}-\frac{2C'^2}{C^2}\right)r_s\frac{\partial}{\partial r_s}-\frac{r_s^2C'^2}{C^2}\frac{\partial^2}{\partial r_s^2}\right\};$$

$$C' = \frac{\partial C}{\partial \psi}, \quad C'' = \frac{\partial^2 C}{\partial \psi^2} \quad \text{and} \quad \dot{C} = \frac{\partial C}{\partial t}.$$

The dimensionless initial condition for the solid-region temperature is:

$$\text{at time } t = 0^+; \quad T_s = 1 \quad \text{at } r_s = 1, \quad \text{and} \quad T_s = 0 \quad \text{for all } r_s, \quad 0 \leqslant r_s < 1. \tag{10b}$$

The dimensionless boundary conditions are:

$$\left.\begin{aligned} &T_s = 1 \quad \text{at } r_s = 1, \\ \text{and} \quad &\frac{1}{C}\left(1+\frac{\Sigma'^2}{\Sigma^2}\right)\frac{\partial T_s}{\partial r_s}+\frac{\Sigma'}{\Sigma^2}\frac{\partial T_s}{\partial \psi} = \frac{Bi}{1+\epsilon K Bi}(1+\Sigma'^2/\Sigma^2)^{\frac{1}{2}}T_s \quad \text{at } r_s = 0. \end{aligned}\right\} \tag{10c}$$

2.6. *Dimensionless formulation for the liquid–solid interface*

The equation for the solid–liquid interface location (1*e*) is non-dimensionalized using appropriate scalings from both liquid and solid regions, (6) and (9). After some rearrangement, this results in a governing equation for Z, called the gap-function equation:

$$2tZ\dot{Z}+Z^2 = Ste\left\{1+\frac{2tZ'}{(1+Z(2t)^{\frac{1}{2}})^2}\right\}\left\{\frac{Sb\,Z(2t)^{\frac{1}{2}}}{1+Z(2t)^{\frac{1}{2}}-\Sigma}\left.\frac{\partial T_s}{\partial r_s}\right|_{r_s=1}-\left.\frac{\partial T_l}{\partial r_l}\right|_{r_l=1}\right\}, \tag{11a}$$

where

$$Ste = \frac{\rho_l}{\rho_s}\frac{c_l(T_i-T_0)}{h_{sl}} \quad \text{(Stefan number)}, \tag{11b}$$

$$Sb = \frac{k_s}{k_l}\frac{T_0-T_\infty}{T_i-T_0} \quad \text{(subcooling number)}. \tag{11c}$$

c_l denotes the specific heat of the liquid PCM.

2.7. *Dimensionaless initial conditions for the liquid region*

The dimensionless initial conditions for the melt region are determined by letting $t = 0^+$ in the governing equations (7) and (11) and the boundary conditions (8). This results in a reduced set of partial differential equations, of which the solution is the initial condition:

$$\frac{\partial^2\omega}{\partial r_l^2}+\frac{r_l Z^2}{Pr}\frac{\partial\omega}{\partial r_l}+\frac{3Z^3\omega}{Pr}+\frac{Z}{Pr}\frac{\partial(\omega,f)}{\partial(r_l,\psi)} = 0; \tag{12a}$$

$$\frac{\partial^2 T_l}{\partial r_l^2}+r_l Z^2\frac{\partial T_l}{\partial r_l}+Z\frac{\partial(T_l,f)}{\partial(r_l,\psi)} = 0; \tag{12b}$$

$$\frac{\partial^2 f}{\partial r_l^2} = -Z^2\omega; \quad \frac{\partial^2 T_s}{\partial r_l^2}+\frac{r_l Z^2}{\lambda}\frac{\partial T_s}{\partial r_l} = 0; \tag{12c–d}$$

$$Z^2 = Ste\left\{Sb\frac{\partial T_s}{\partial r_l}-\frac{\partial T_l}{\partial r_l}\right\}\Bigg|_{r_l=1}; \tag{12e}$$

subject to the boundary conditions:

$$T_l = 1, \quad f = 0, \quad \omega = -\frac{1}{Z^2}\frac{\partial^2 f}{\partial r_l^2} \quad \text{at } r_l = 0; \tag{12f}$$

$$T_l = 0, \quad \frac{\partial f}{\partial\psi} = -u_R, \quad \omega = -\frac{1}{Z^2}\frac{\partial^2 f}{\partial r_l^2}, \quad T_s = 1 \quad \text{at } r_l = 1; \tag{12g}$$

$$T_s \to 0 \quad \text{as } r_l \to \infty, \tag{12h}$$

where $u_R = Z(1-\Delta)$. Note that (12) are only first order in ψ.

If there is no density change upon melting ($\Delta = 1$), then the initial condition becomes simple enough to determine analytically. There is no initial fluid motion and the ψ dependence drops out of (12), resulting in ordinary differential equations. The solution is:

at $t = 0^+$ (infinitesimal melt region exists);

$$T_l = 1-\operatorname{erf}\{r_l Z/2^{\frac{1}{2}}\}\operatorname{erf}\{Z/2^{\frac{1}{2}}\}, \quad \omega \equiv f \equiv 0, \tag{13a, b}$$

$$T_s = 1-\frac{\operatorname{erf}\{r_l Z/(2\lambda)^{\frac{1}{2}}\}-\operatorname{erf}\{Z/(2\lambda)^{\frac{1}{2}}\}}{\operatorname{erfc}\{Z/(2\lambda)^{\frac{1}{2}}\}}, \tag{13c}$$

$$Z = \left(\frac{2}{\pi}\right)^{\frac{1}{2}} Ste\left\{\frac{e^{-\frac{1}{2}Z^2}}{\operatorname{erf}\{Z/2^{\frac{1}{2}}\}}-\frac{(Sb/\lambda^{\frac{1}{2}})\,e^{-Z^2/2\lambda}}{\operatorname{erfc}\{Z/(2\lambda)^{\frac{1}{2}}\}}\right\}. \tag{13d}$$

Initial condition (13*d*) needs to be solved iteratively; once the initial Z value has been determined, the initial values for T may be computed. Equations (13*a*, *c*, *d*) are the analytical solution as first determined by Stefan and Neumann (Carslaw & Jaeger 1962; Rubenstein 1971).

With the exception of boundary conditions in ψ, (6)–(13) now provide a complete formulation of the problem. In the present case, symmetry boundary conditions are used:

$$\frac{\partial T}{\partial \psi} = 0, \quad f = \omega = 0 \quad \text{at } \psi = 0°, 180°. \tag{14}$$

For large values of Ra, of order 10^5 to 10^6, an unsteady oscillating motion of the thermal plume may develop (Bathelt *et al.* 1979; Goldstein & Ramsey 1979; Sparrow *et al.* 1978). The value of $Ra = 37500$, used in the present numerical computations, is low enough that the symmetry boundary condition (14) is justified. The numerical method could be modified to determine solutions for large values of Ra by extending the computational domain to the whole unit circle, from $\psi = 0°$ to 360°. The symmetry conditions along $\psi = 0°$ and 180° would then be replaced by matching the dependent variables at $\psi = 0°$ and 360°.

3. Results and discussion

Three main cases are examined and compared with each other in order to discern clearly the effects of subcooling and density change on the heat-transfer rates, melting rates and flow fields. In all three cases $Ste = 0.02$, $Ra = 37500$, $Pr = 50$ and $\lambda = 1$. These values are typical for a melting problem using paraffin for the PCM. Bi is set equal to 1. This value is typical for natural convection along the outside of the container. The thermal conductivity of the container-wall material is assumed to be much greater than that of the solid PCM, $K = 0.01$. This is reasonable for metallic containers. Finally, the shape of the container is specified as a circular cylinder with $\Sigma = 3$ and $\epsilon = 0.01$. Each of the three cases uses the preceding values of dimensionless parameters: only Sb and Δ are changed in each case:

$$\begin{aligned} &\text{Case 1:} \quad Sb = 0, \quad \Delta = 1, \\ &\text{Case 2:} \quad Sb = 1, \quad \Delta = 1, \\ &\text{Case 3:} \quad Sb = 0, \quad \Delta = 1.1. \end{aligned}$$

The first case represents the control for comparison purposes. In the second case, $Sb = 1$ indicates a strong subcooling effect. The solid is initially subcooled below the melting temperature by the amount by which the heated cylinder surface is above the melting temperature (approximately). In case 3, $\Delta = 1.1$ indicates that the solid PCM is 10% denser than the liquid phase. This magnitude of change is typical for paraffins, such as *n*-octadecane.

3.1. *Subcooling effect*

The main effect of subcooling – a decrease in melting rate – is clearly demonstrated in figure 2. Here the melt regions for $Sb = 0$ and $Sb = 1$ are compared at a dimensionless time of 14.1. The location of the liquid–solid interface can be calculated from the liquid-region gap function:

$$\frac{R}{a} = 1 + Z(2t)^{\frac{1}{2}}. \tag{15}$$

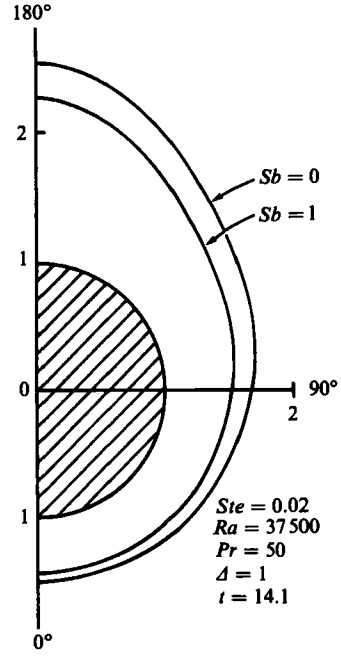

FIGURE 2. Decrease in growth of the melt region due to subcooling effect.

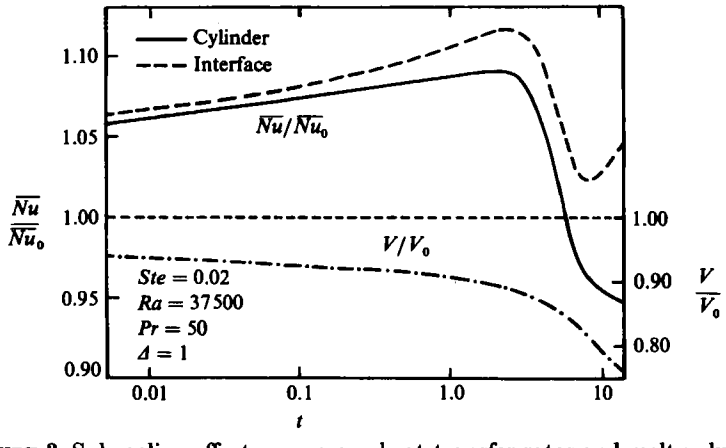

FIGURE 3. Subcooling effect on average heat-transfer rates and melt volume.

Since the subcooled solid requires some sensible-heat gain in order to raise it to the melting temperature, less thermal energy is available for melting. Additional energy is lost because it is conducted completely through the solid PCM, and convected away into the ambient atmosphere. The net result is that the subcooled case has a melt region which is 23 % smaller by volume.

Figure 3 gives additional evidence in support of this interpretation. It gives the ratio of the dimensionless volumes of the melt region for the cases $Sb = 0$ and $Sb = 1$. These volumes are denoted V_0 and V respectively, and are determined by the volume integration:

$$\bar{V} = \frac{1}{\pi}\int_0^{\pi} [1 + Z(2t)^{\frac{1}{2}}]^2 \, d\psi - 1. \tag{16}$$

The volume ratio is less than one and decreases with time. At around $t = 3$, increased thermal losses to the ambient atmosphere cause the curve to drop more sharply. This sudden drop may also be due, in part, to natural convection which becomes the dominant mode of heat transfer at about this point. The magnitude of natural convection is proportional to the Rayleigh number which uses the width of the melt region as a lengthscale (Yao & Chen 1980). Since the subcooled melt region is smaller than in the case which is not subcooled, natural convection is weaker in the subcooled case. Figure 3 also gives information on the average dimensionless heat-transfer rates along the heated cylinder and liquid–solid interface. They are denoted by $\overline{Nu_i}$ and $\overline{Nu_m}$, respectively, and are determined by integrating the local dimensionless heat-transfer rates along the cylinder and interface:

$$\overline{Nu_i} = \frac{1}{\pi}\int_0^\pi Nu_i \,\mathrm{d}\psi; \tag{17a}$$

and

$$\overline{Nu_m} = \frac{1}{\pi F_1}\int_0^\pi Nu_m[1+Z(2t)^{\frac{1}{2}}]\,\mathrm{d}\psi; \tag{17b}$$

where

$$Nu = \frac{qa}{k(T_i - T_0)} \quad \text{(local Nusselt number)}, \tag{17c}$$

and

$$F_1 = \frac{1}{\pi}\int_0^\pi \{1+Z(2t)^{\frac{1}{2}}\}\left\{1+\frac{Z'^2}{(Z+(2t)^{-\frac{1}{2}})^2}\right\}^{\frac{1}{2}}\mathrm{d}\psi. \tag{17d}$$

Physically, F_1 is the average dimensionless radius R_{ave}/a, for the liquid–solid interface. Figure 3 compares these dimensionless average heat-transfer rates with the $Sb = 0$ case by plotting the ratio $\overline{Nu}/\overline{Nu_0}$. $\overline{Nu_0}$ is the corresponding dimensionless heat-transfer rate along the cylinder or interface for the $Sb = 0$ case.

Consider $\overline{Nu}/\overline{Nu_0}$ for the interface. At first, this ratio is seen to be greater than one and steadily increasing. The average heat-transfer rate is greater with subcooling than without it. This effect, also observed by Yao & Cherney (1981), is interesting because the melt volume is lessened by subcooling. Apparently the thermal energy used for solid sensible-heat gain contributes enough to $\overline{Nu_m}$ to more than make up for the reduced latent-heat gain. The increase in average heat-transfer rates makes sense if one considers the simple electrical analogy – subcooling increases the overall thermal potential to $T_i - T_\infty$. The monotone increase in $\overline{Nu}/\overline{Nu_0}$ along the interface is abruptly terminated at about $t = 3$, when natural convection becomes the dominant mode of heat transfer. In the subcooled case, natural convection is weaker and, corresponding to this, the heat transfer drops off. At about $t = 8$, the ratio bottoms out at a value still larger than one and begins to rise again. At this point, the natural-convection flow field in the subcooled case has matured, and is now asymptotically approaching the case of natural convection about a horizontal cylinder in an infinite fluid.

The behaviour of the dimensionless heat-transfer ratio for the cylinder surface is quite similar. The only qualitative difference occurs near $t = 8$, when the natural-convection flow field matures. Here, the ratio keeps on decreasing, although not as rapidly as in the early convection stage. This is in marked contrast to the heat-transfer ratio for the interface, which increases.

Thermal energy enters the melting system along the cylinder surface. The total dimensionless energy which enters is denoted by $E1$. It may be determined by integrating the average heat-transfer rate along the cylinder surface in time:

$$E1 = 2\,Ste\int_0^t \overline{Nu_i}\,\mathrm{d}t. \tag{18a}$$

Here $\overline{Nu_i}$ is given by (17*a*). The choice of characteristic scale for energy is the amount of energy required to melt a volume of solid (at the melting temperature) equal to the volume of the heated cylinder. For example, if $Sb = 0$ and there is no liquid sensible-heat gain, when $E1 = 1$ then $V = 1$ also. With the choice of characteristic scale for energy, the latent-heat storage is easily evaluated in dimensionless form. Denoted by $E2$, it is:

$$E2 = V. \tag{18b}$$

The liquid sensible-heat gain, denoted by $E3$, can be found using a volume integration to determine the excess thermal energy in the liquid:

$$E3 = \frac{2}{\pi} Ste \int_0^{\pi} \int_0^1 Z(2t)^{\frac{1}{2}} [1 + r_1 Z(2t)^{\frac{1}{2}}] T_1 \, dr_1 \, d\psi. \tag{18c}$$

The solid sensible-heat gain, denoted by $E4$, can be found in similar fashion:

$$E4 = \frac{2}{\pi} \frac{Ste\, Sb}{\lambda} \int_0^{\pi} \int_0^1 C(\Sigma - Cr_s) \, T_s \, dr_s \, d\psi. \tag{18d}$$

Finally, energy may leave the system by convection on the outside of the container wall. Denoted by $E5$, this energy loss may be determined in dimensionless form by:

$$E5 = 2F_2 Ste \int_0^t \overline{Nu_w} \, dt, \tag{18e}$$

where

$$\overline{Nu_w} = \frac{1}{\pi F_2} \int_0^{\pi} \Sigma \, Nu_w \, d\psi,$$

$$Nu_w = Sb \left\{ \frac{1}{C} \left(1 + \frac{\Sigma'^2}{\Sigma^2} \right) \frac{\partial T_s}{\partial r_s} + \frac{\Sigma'}{\Sigma^2} \frac{\partial T_s}{\partial \psi} \right\} \Bigg|_{r_s = 0}$$

(local dimensionless heat-transfer rate at the container wall),

and

$$F_2 = \frac{1}{\pi} \int_0^{\pi} \Sigma \left[1 + \frac{\Sigma'^2}{\Sigma^2} \right]^{\frac{1}{2}} d\psi.$$

F_2 is an average dimensionless radius S_{ave}/a for the inside surface of the container.

Note that $E1 = E2 + E3 + E4 + E5$ (assuming that the sensible-heat gain of the container wall is negligible), and that this sum may be used as an energy-balance check for the numerical method. Since the governing equations are formulated in non-conservative form, an energy balance provides a real check for the global truncation error of the method. In the actual computations the energy balance remained within 1.5 % of unity.

Figure 4 shows the transient response of the melting system in terms of sensible- and latent-heat storage. The latent-heat storage E_2 is seen to be only slightly less than the total energy input to the system E_1. E_2 is about 85 % of E_1 initially, and then slowly decreases to 75 % of E_1 by $t = 14.1$. The sensible-heat gain of the solid PCM E_4 involves an order of magnitude less thermal energy. Initially, E_4 is about 13 % of E_1 – it makes up the bulk of the difference between $E1$ and $E2$, but note that $E4$ levels off at about $t = 3$. At this point, the melt region is growing fast enough so that the increase in $E4$ due to rising solid temperature is offset by a decrease due to reduced solid volume. The net effect is that $E4$ drops off to about 3 % of E_1 by $t = 14.1$. The liquid-PCM sensible-heat gain $E3$ is seen only briefly in the lower right corner. $E3$ involves two orders of magnitude less thermal energy than $E1$. The liquid sensible-heat gain never accounts for more than 0.8 % of the total energy at any time. This indicates

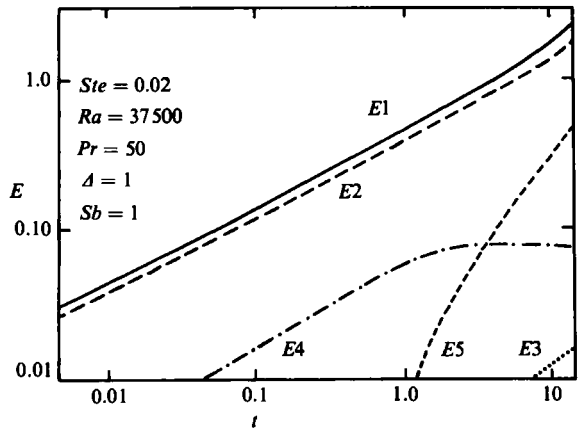

FIGURE 4. Variation of sensible- and latent-heat storage with time when subcooling effect is present.

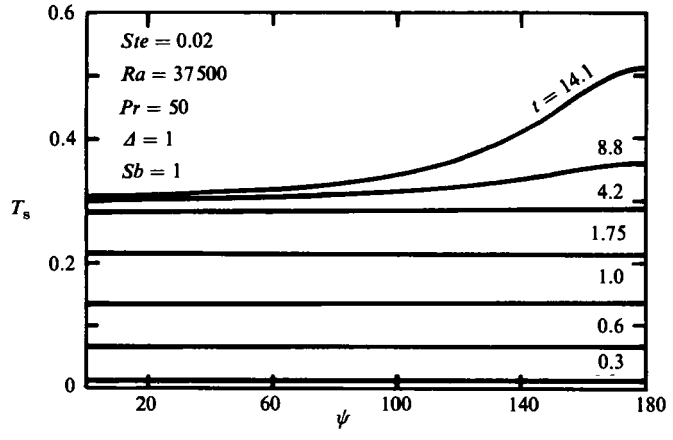

FIGURE 5. Solid PCM temperature along container wall.

the great efficiency of natural-convection heat transfer. For $Ra < 37500$, it is anticipated that $E3$ will become more significant. For $Ra > 37500$, the liquid sensible-heat storage is negligible. The convection heat loss on the outside surface of the container is insignificant until a dimensionless time of 0.1 is reached. Before this time, thermal energy from the heated cylinder has not yet reached any portion of the container wall. The solid-PCM temperature near the wall is still essentially at the original subcooled temperature T_∞. By $t = 0.3$, enough energy has penetrated to the container wall to raise the solid-PCM temperature there by 1%. This is enough to cause a convection loss of about 0.03% of $E1$. The convection loss increases very rapidly as the solid warms up. $E5$ accounts for 1.4% of $E1$ at $t = 1$, and about 21% of $E1$ at $t = 14.1$. At this point, the outer convection loss is so severe that the latent-heat storage of the system is reduced significantly.

Figure 5 shows the temperature response of the solid with time. It gives the dimensionless solid temperature along the container wall, at $r_s = 0$. In figure 5, $T_s = 0$ corresponds to the original subcooled temperature, while $T_s = 1$ corresponds to the melting temperature. Note that temperatures at interior points in the solid PCM (for

$r_s > 0$) will be greater. As mentioned in the discussion of figure 4, negligible thermal energy has penetrated to the container wall before $t = 0.1$. By $t = 0.3$, enough energy has reached the wall to raise the solid-PCM temperature by 1 %. After this point, the temperature increases rapidly with time. The temperature profiles remain quite uniform up to a time of 4.2. For later times, the solid-PCM temperature is noticeably warmer at $\psi = 180°$ than at $\psi = 0°$. This difference becomes quite large by $t = 14.1$. The uniform profiles result because conduction is initially the dominant mode of heat transfer in the melt region. This produces uniform local heat-transfer rates and an annular melt region (Prusa & Yao 1984*a*, *b*). By $t = 3$, natural convection has become the dominant mode of heat transfer in the melt region. A thermal plume forms above the heated cylinder. The local heat-transfer rate along the interface becomes very large at $\psi = 180°$, above the cylinder, and very small at $\psi = 0°$, below the cylinder. As a result, solid PCM above the cylinder gets warmer and melts sooner than solid material elsewhere in the system. It is natural convection which causes the non-uniform temperature profiles in figure 5. Note that, although convection becomes the dominant mode of heat transfer in the liquid by $t = 3$, the temperature profile at $r_s = 0$ does not become appreciably skewed until $t = 8.8$. This is due to a thermal inertia effect: it takes the non-uniform energy flow that long to travel through the solid PCM from the liquid–solid interface to the container wall.

3.2. *Density-change effect*

The effect of density change on the melting process is most pronounced very early in the conduction stage. All effects decrease very rapidly with time for the case $\Delta = 1.1$, when compared with the standard case where $\Delta = 1.0$. The effects which are most notable involve the flow field. Surprisingly, almost no effect was observed on the temperature field or heat-transfer rates, which are observed always to be within 0.02% of each other. Since detailed information on the temperature fields and heat-transfer rates is given in Prusa & Yao (1984*b*), the information is not repeated here.

Our surprising numerical result is supported by an order-of magnitude analysis of the early convection effect on the heat-transfer problem. From (12*b*) and the definition of the stream function, it can be shown that the convection effect due to density change is $O(Z^2(1-\Delta))$. From the numerical result, it appears that the initial value of Z is not affected by density change (at least for case 3). Consequently, the initial value of Z is still given by (13*d*), which when expanded in a power series has a leading term of $Ste^{\frac{1}{2}}$. We then conclude that, for early times, for values of Ste which are not large:

$$Z\frac{\partial(T_1, f)}{\partial(r_1, \psi)} \sim O[Ste(1-\Delta)]. \tag{19}$$

Apparently, a significant early convection effect on heat transfer can be expected only for large Ste and values of Δ appreciably different from unity. Further support of this conclusion comes from an integral solution (Prusa 1985). The integral method incorporates the effects of density change in a one-dimensional melting problem. It predicts the same result as (19).

Because the specific volume of the liquid is greater than that of the solid PCM, for $\Delta = 1.1$, the melting process introduces excess fluid volume into the melt region. This excess volume cannot remain in the melt region because the fluid is modelled as being incompressible. In order to allow the excess volume to escape, a 'hole' is introduced into the melt region. This opening appears as a natural consequence of the

stream-function boundary condition (8*b*) along $r_1 = 1$. The symmetry BC (14) requires that no fluid can flow across the rays $\psi = 0°$, 180°. Since the heated cylinder is impermeable, the stream function must be the same constant on all three boundaries. But (8*b*) indicates that f either increases ($\Delta > 1$) or decreases ($\Delta < 1$) along the liquid–solid interface. (This non-uniform stream function BC has a precedent in boundary-layer theory with suction, see Schlichting (1979).) This means that a discontinuity in the value of f must occur somewhere along the interface. The physical meaning of this discontinuity can be understood with the following argument. Let $\bar{f}_2 - \bar{f}_1 = \int_R \mathrm{d}\bar{f}$ denote the change in streamfunction across the discontinuity (the line integral is evaluated along the interface). The integral can be expressed in terms of the components:

$$\int_R \mathrm{d}\bar{f} = \int_{\bar{\psi}} \frac{\partial \bar{f}}{\partial \bar{r}} \mathrm{d}\bar{r} + \int_{\bar{r}} \frac{\partial \bar{f}}{\partial \bar{\psi}} \mathrm{d}\bar{\psi}, \tag{20a}$$

where the first integral on the r.h.s. is evaluated along a line of constant $\bar{\psi}$, and the second integral is evaluated along a line of constant $\bar{r}$. Now, from the definition of streamfunction, one obtains:

$$\int_R \mathrm{d}\bar{f} = \int_{\bar{\psi}} \bar{v}\, \mathrm{d}\bar{r} - \int_{\bar{r}} (\overline{ru})\, \mathrm{d}\bar{\psi}. \tag{20b}$$

Clearly, these two integrals on the r.h.s. give a volume flow rate across the line of integration. Consequently, the stream-function discontinuity is a hole through which fluid may escape (or enter if $\Delta < 1$). The choice for the location of the hole, or holes, is arbitrary. In the present study, we have set it at the top of the melt region, at $\psi = 180°$. This position corresponds to the location of a tube or slot sometimes placed in an experimental melting system in order to allow excess fluid to leave the melt region (Gau & Viskanta 1984). Since the fluid motion induced by density change has negligible effect on the heat-transfer problem, the location of the hole appears to be an unimportant factor in this aspect of the melting problem. Note that this negligible effect also means that the loss of fluid from the melt region does not seriously disturb the energy balance described in the preceding section. In fact, as long as the hole is located on the solid–liquid interface, escaping fluid is at the melting temperature T_0, and has no sensible heat to carry away. There is no effect at all on the energy balance. But even if the hole is located on the heated cylinder (a hole could be drilled through its surface and excess fluid drained through it), so that the escaping fluid is at the temperature T_i, the thermal loss would still be negligible. This result is indicated by the integral solution (Prusa 1985). In the integral method, excess fluid can escape only through the heated surface, which is permeable. Consequently, the fluid escapes from the melt region with the maximum sensible heat possible. This boundary condition was chosen so that the effects of density change on the heat-transfer problem would be exaggerated as much as possible. Despite this exaggerated boundary condition, for $Ste = 0.02$ and $\Delta = 1.1$, the integral method predicts a decrease in melting rate of only 0.05%. Furthermore the integral method predicts that, in the range $0 < Ste \leqslant 1$, the maximum change in melting rate (compared to the $\Delta = 1$ case) is bounded by:

(i) 2.0% for $0.9 \leqslant \Delta \leqslant 1.1$ and (ii) 10.0% for $0.55 \leqslant \Delta \leqslant 1.60$.

The location of the hole does have an overwhelming influence on the initial flow field, however. The variation of average dimensionless shear stresses along the heated

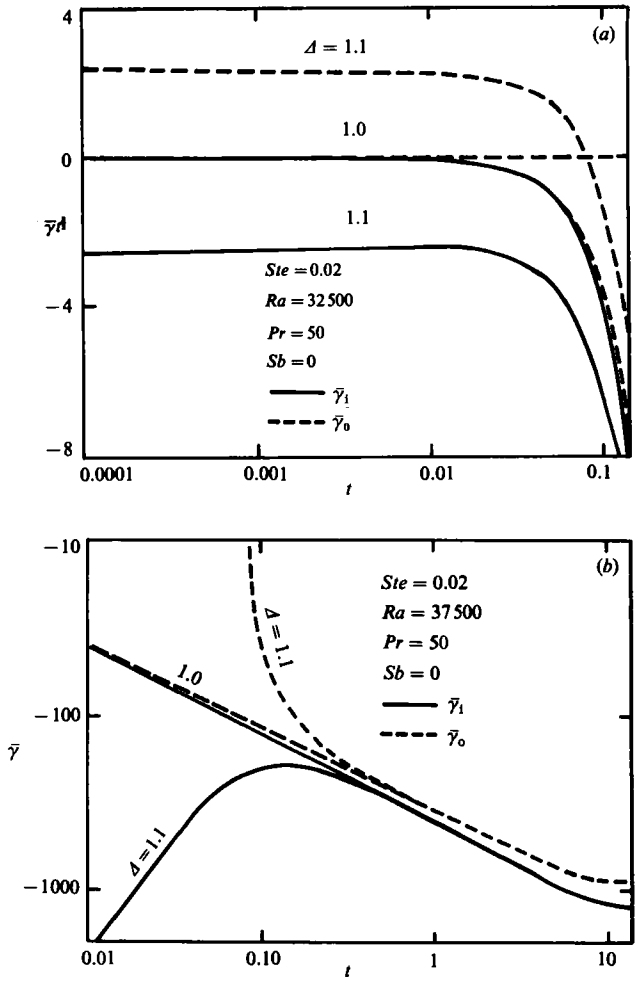

FIGURE 6. Density-change effect on average shear stresses: (*a*) average shear stresses early in the melting process when conduction is the dominant mode of heat transfer; (*b*) average shear stresses late in the melting process when natural convection is the dominant mode of heat transfer.

cylinder and liquid–solid interface with time are shown in figure 6. They are denoted by $\overline{\gamma_i}$ and $\overline{\gamma_o}$, respectively, and are determined from:

$$\overline{\gamma_i} = -\frac{1}{\pi(2t)^{\frac{1}{2}}}\int_0^{\pi}\frac{1}{Z^2}\frac{\partial^2 f}{\partial r_1^2}\bigg|_{r_1=0}\mathrm{d}\psi; \tag{21a}$$

and

$$\overline{\gamma_o} = -\frac{1}{\pi F_1(2t)^{\frac{3}{2}}}\int_0^{\pi}\frac{1+Z(2t)^{\frac{1}{2}}}{Z^2}\left\{1+\frac{Z'^2}{[Z+1/(2t)^{\frac{1}{2}}]^2}\right\}^{-\frac{1}{2}} \times\left\{1+\frac{2Z'^2}{[Z+1/(2t)^{\frac{1}{2}}]^2}+\frac{Z'^4}{[Z+1/(2t)^{\frac{1}{2}}]^4}\right\}\frac{\partial^2 f}{\partial r_1^2}\bigg|_{r_1=1}\mathrm{d}\psi \tag{21b}$$

Note that the shear stresses become unbounded like $t^{-\frac{3}{2}}$ as $t\to 0$.

From figure 6(*a*), it can be seen that $\overline{\gamma_i}\,t^{\frac{3}{2}}$ and $\overline{\gamma_o}\,t^{\frac{3}{2}}$ approach constants of equal but opposite magnitudes as $t\to 0$. This behaviour can be explained by interpreting

the average shear stresses in terms of the velocity field. Note that (21*a*, *b*) collapse into

$$\overline{\gamma_1} = -\frac{1}{2tZ\pi}\int_0^{\pi} \left.\frac{\partial v}{\partial r_1}\right|_{r_1=0} \mathrm{d}\psi, \tag{21c}$$

and

$$\overline{\gamma_0} = -\frac{1}{2tZ\pi}\int_0^{\pi} \left.\frac{\partial v}{\partial r_1}\right|_{r_1=1} \mathrm{d}\psi, \tag{21d}$$

as $t \to 0$. Along $r_1 = 0$, $v = 0$ (no-slip BC) and along $r_1 = 1$, $v = 0$ again. $v = 0$ along $r_1 = 1$ because for the blowing BC, $v_R \propto Z'$. From the numerical result $Z' = 0$ at $t = 0$. Since excess fluid volume produced by melting must move out through the 'opening' at $\psi = 180°$, $v > 0$ on average. Since $v = 0$ at $r_1 = 0, 1$, symmetric unimodal velocity profiles are produced. This causes the velocity gradients in (21*c*, *d*) to approach values which are of equal but opposite magnitudes as $t \to 0$. This simple initial fluid motion begins to become modified significantly for $t > 0.01$. This is indicated in figure 6(*a*) by the average shear stresses dropping off sharply for $t > 0.01$. The drop-off is caused by natural convection, which becomes significant for $t > 0.01$. By $t = 0.1$, natural convection has become as strong an effect on the fluid motion as the density change. At $t = 1$, natural convection has become a much stronger effect, while the density-change effect has continued to decrease like $t^{-\frac{3}{4}}$ as $t \to \infty$. The effect of natural convection with density change is indicated by the $\Delta = 1.0$ curve. This curve approaches zero asymptotically from below as $t \to 0$.

Although figure 6(*a*) clearly shows the early behaviour of the average dimensionless shear stress, it does not clearly indicate that for $\Delta = 1.1$, $\overline{\gamma_1}$ and $\overline{\gamma_0}$ are rapidly converging to the $\overline{\gamma_1}$ and $\overline{\gamma_0}$ values for the $\Delta = 1.0$ case. This is clearly seen in figure 6(*b*), which uses $\bar{\gamma}$ rather than $\bar{\gamma}t^{\frac{3}{4}}$ as the vertical coordinate. By $t = 1.0$, the average shear stresses for the two cases are within 1 % of each other. Since the only perceptible effect of density change appears to be in the flow field, the $\Delta = 1.1$ calculation is terminated at this point. For $t > 1.0$, there will be only a negligible difference when compared to the $\Delta = 1.0$ case.

Figure 7 presents more detailed information on the effects of density change on the flow field. It gives velocity profiles for the angular component of velocity v along selected rays of constant ψ. The dimensionless time is $t = 0.1$, which is still early in the melting process. Conduction is overwhelmingly the dominant mode of heat transfer. The annular melt region is greatly expanded in figure 7, the true position of the liquid–solid interface being indicated by the dashed boundary. The density-change effect has decayed enough while the natural-convection effect has increased enough so that both factors are roughly of comparable magnitude at $t = 0.1$. This can be observed from the velocity profiles. Natural convection will act to produce S-shaped velocity profiles, with $v > 0$ near the heated cylinder and $v < 0$ near the interface. This is due to the vortex circulation induced by buoyancy force. Fluid rises along the heated cylinder, and descends along the interface. Recall that density change will act to produce symmetric unimodal velocity profiles, with $v > 0$. The interaction between these two effects produces the profiles seen in figure 7. The v profile at $\psi = 33.5°$ is closest to the pure natural-convection profile, while the profile at $\psi = 166.8°$ is closest to the pure density-change profile. As ψ increases from 0, more and more excess volume is being added locally due to melting. As a result, the fluid must move towards the top at increasing speeds in order to conserve volume locally. Eventually, the density change overwhelms the buoyancy effect. Later on in the melting process, this density-change effect will have decayed greatly, while

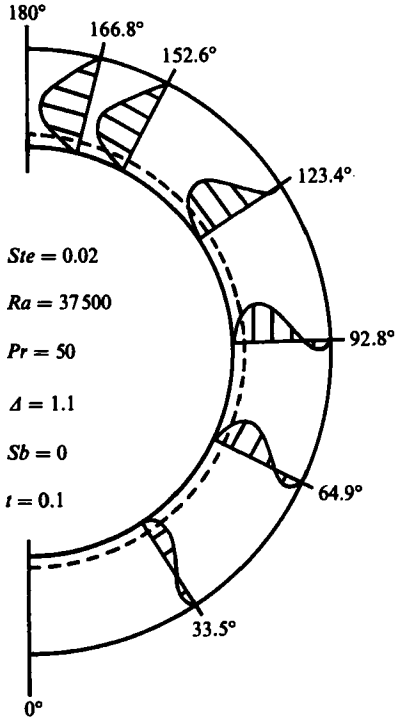

FIGURE 7. Density-change effect on angular component of velocity.

natural convection will have increased greatly. All velocity profiles will look like pure natural-convection profiles. The density effect will be only a minor perturbation. The one exception will be in a very small region – the local neighbourhood of the hole.

4. Conclusions

Subcooling is found to decrease substantially the latent-heat storage of the melting system. However, the solid sensible-heat gain can be enough to completely offset this loss. Consequently, subcooling can actually increase the overall rate of heat transfer and the overall energy storage. The liquid sensible-heat gain is found to be negligible for $Ra > 37500$. A large energy loss due to convection along the outside surface of the container was observed, surprisingly with a very modest value of convection coefficient (corresponding to natural convection).

Density effect upon melting is found to have a negligible effect on the temperature field and heat-transfer rates in the melting problem. In an incompressible-fluid model, it does introduce tremendous fluid motion in the beginning of the melting process, as excess fluid rushes out of the melt region (for $\Delta > 1$) through the hole in the interface. As $t \to 0$, the magnitude of the fluid motion becomes unbounded. As $t \to \infty$, this magnitude decreases (like t^{-1} in the case of v, the angular velocity component) and approaches zero asymptotically. At the same time, fluid motion induced by buoyancy force increases as $t \to \infty$. Early in the melting process, a point is reached where the two effects are roughly of the same magnitude. Beyond this time, natural convection soon overwhelms the effects of density change, which then become negligible.

REFERENCES

BATHELT, A. G., VISKANTA, R. & LEIDENFROST, W. 1979 An experimental investigation of natural convection in the melted region around a heated horizontal cylinder. *J. Fluid Mech.* **90**, 227–239.

CARSLAW, H. S. & JAEGER, J. C. 1962 *Conduction of Heat in Solids*, 2nd edn. pp. 282–296. Oxford University Press.

EPSTEIN, M. & CHEUNG, F. B. 1983 Complex freezing–melting interfaces in fluid flow. *Ann. Rev. Fluid Mech.* **15**, 293–319.

GAU, C., & VISKANTA, R. 1984 Melting and solidification of a metal system in a rectangular cavity. *Intl J. Heat Mass Transfer* **27**, 113–123.

GOLDSTEIN, R. J. & RAMSEY, J. W. 1979 Heat transfer to a melting solid with applications to thermal energy storage systems. *Heat Transfer Studies: Festschrift for E. R. G. Eckert*, pp. 199–208. Hemisphere.

HO, C. J. & VISKANTA, R. 1982 Experimental study of melting in a rectangular cavity. In *Proc. 7th Intl Heat Transfer Conf., München, Fed. Rep. of Germany* **2**, 369–374.

PRUSA, J. 1983 A spatial Stefan problem modified by natural convection: melting around a horizontal cylinder. Ph.D. dissertation, University of Illinois at Urbana-Champaign.

PRUSA, J. 1985 An integral solution incorporating the effects of density change and subcooling for a one dimensional melting problem. *Tech. Rep. ISU-ERI-AMES-85153.*

PRUSA, J. & YAO, L. S. 1984*a* Melting around a horizontal heated cylinder: part I – perturbation and numerical solutions for constant heat flux boundary condition. *Trans. ASME* C: *J. Heat Transfer* **106**, 376–384.

PRUSA, J. & YAO, L. S. 1984*b* Melting around a horizontal heated cylinder: part II – numerical solution for isothermal boundary condition. In *Proc. ASME/JSME Thermal Engng Joint Conf., March 20–24, 1984, Honolulu, Hawaii; Trans. ASME* C: *J. Heat Transfer* **106**, 469–472.

RAMACHANDRAN, N., GUPTA, J. P. & JALURIA, Y. 1982 Thermal and fluid flow effects during solidification in a rectangular enclosure. *Intl J. Heat Mass Transfer* **25**, 187–193.

RIEGER, H., PROJAHN, U. & BEER, H. 1982 Analysis of the heat transport mechanisms during melting around a horizontal circular cylinder. *Intl J. Heat Mass Transfer* **25**, 137–147.

ROACHE, P. 1976 *Computational Fluid Dynamics* (revised printing), pp. 139–141. Hermosa.

RUBENSTEIN, L. T. 1971 The Stefan Problem. *Trans. Math. Monographs* **27**, 1–15.

SAITOH, T. & HIROSE, K. 1982 High Rayleigh number solutions to problems of latent heat thermal energy storage in a horizontal cylinder capsule. *Trans. ASME* C: *J. Heat Transfer* **104**, 545–553.

SCHLICHTING, H. 1979 *Boundary Layer Theory*, 7th edn, pp. 383–391. McGraw-Hill.

SPARROW, E. M., PATANKAR, S. V. & RAMADHYANI, S. 1977 Analysis of melting in the presence of natural convection in the melt region. *Trans. ASME* C: *J. Heat Transfer* **99**, 520–526.

SPARROW, E. M., SCHMIDT, R. R. & RAMSEY, J. W. 1978 Experiments on the role of natural convection in the melting of solids. *Trans. ASME* C: *J. Heat Transfer* **100**, 11–16.

YANG, K. T. 1972 Formation of ice in plane stagnation flow. *Appl. Sci. Res.* **17**, 377–396.

YAO, L. S. & CHEN, F. F. 1980 Effects of natural convection in the melted region around a heated horizontal cylinder. *Trans. ASME* C: *J. Heat Transfer* **102**, 667–672.

YAO, L. S. & CHERNEY, W. 1981 Transient phase-change around a horizontal cylinder. *Intl J. Heat Mass Transfer* **24**, 1971–1981.